Finite Element Modeling of Microstructural Changes in Hard Machining of SAE 8620

Serafino Caruso [1,*], Giovanna Rotella [2], Antonio Del Prete [3] and Domenico Umbrello [1]

[1] Department of Mechanical, Energy and Management Engineering, University of Calabria, CS 87036 Rende, Italy; domenico.umbrello@unical.it

[2] Department of Computer Engineering, Modeling, Electronics and Systems Engineering, University of Calabria, CS 87036 Rende, Italy; giovanna.rotella@unical.it

[3] Department of Engineering for Innovation, University of Salento, Via per Monteroni, 73100 Lecce, Italy; Antonio.delprete@unisalento.it

* Correspondence: serafino.caruso@unical.it; Tel.: +39-0984-494147

check for updates

Abstract: Surface and subsurface microstructural characterization after machining operations is a topic of great interest for both academic and industrial research activities. This paper presents a newly developed finite element (FE) model able to describe microstructural evolution and dynamic recrystallization (DRX) during orthogonal hard machining of SAE 8620 steel. In particular, it predicts grain size and hardness variation by implementing a user subroutine involving a hardness-based flow stress and empirical models. The model is validated by comparing its output with the experimental results available in literature at varying the cutting speed, insert geometry and flank wear. The results show a good ability of the customized model to predict the thermo-mechanical and microstructural phenomena taking place during the selected processes.

1. Introduction

Hard machining involves a series of surface and subsurface structural changes that need to be controlled avoiding unwanted detrimental effects on product quality [1,2]. These modifications occur because of severe plastic deformation [3] and localized rapid thermo-mechanical work [4] resulting in grain refinement and phase transformation. Thus, machined surface and subsurface can show significantly different microstructure from the bulk material. Since this important aspect (laying to the field of surface integrity) directly influences the functional performance of machined components, it needs to be carefully investigated and analyzed. Therefore, it is useful to have accurate constitutive models to describe the material behavior depending on strain, strain rate, temperature, hardness, grain size, phase transformation, etc., especially in the deformation zones.

Cutting processes involve high strain, strain rate and temperatures leading to a complex thermo-mechanical effects which are mainly modeled and described by two types of equations: phenomenological equations (based on empirical functions of the investigated variables) [5–8] and physically-based equations (involving microscale physical aspects) [9–11]. Although physically-based models can accurately describe the material response by considering the microstructural aspect of the plastic deformation, their implementation is limited due to their complexity and the difficulty in identifying the needed parameters. Thus, empirical models are still widely used and preferred.

Among the empirical equations, the Johnson–Cook (J–C) model [5] is the most commonly employed in modeling and simulations for its simple form. In fact, it is widely used even for other

material systems such as fiber reinforced composites [12]. It is a thermo-elastic–visco-plastic material constitutive model describing the flow stress as a product of strain, strain rate and temperature. However, it is inaccurate at high strain rates and does not account for material softening at high strains and temperatures, typical of the severe plastic deformation processes as hard turning machining; several modified forms were developed to overcome these limitations.

Lin et al. [13] combined the Zerilli–Armstrong (Z–A) model and J–C equation to provide a more accurate and precise estimation of the flow stress for the typical high-strength alloy steel.

Calamaz et al. [6] modified the J–C model to predict the softening effect at large strains and temperatures, by considering second order interactions of strain, strain rate and temperature, and allowing shear banding to be simulated without a failure damage criterion.

Ozel et al. [14] proposed a modified J–C material model that includes the temperature-dependent flow softening effect in addition to strain and strain rate hardening and thermal softening effects.

Li et al. [15] proposed a modified J–C model to describe the quasi-static stress–strain responses over a wider temperature range for as-quenched AA2219 (Al–Cu–Mn alloy).

Le et al. [16] developed a modified J–C model to predict the flow stress behavior of commercial pure titanium to determine the quantitative variation of the strain rate sensitivity and the strain hardening with temperature.

Tan et al. [17] modified the original J–C model considering the constant C as nonlinear relations with strains and strain rates for 7050-T7451 aluminum alloy.

Wang et al. [18] established a new J–C model by modifying the constant C as sine function with strain rates and temperatures, improving the prediction accuracy for higher strain rates for Inconel 718 cutting processes.

Constitutive J–C models of machining work material are also coupled with internal variables to consider the evolution of the dislocation density, hardness, grain size, phase transformation, etc. with deformation.

Rotella et al. [19] modeled the flow softening effect taking place during machining processes, such as dynamic recrystallization, by introducing in a modified J–C model a variable that represents the evolution of the grain size during the process.

Umbrello et al. [20] modified the original J–C equation introducing the hardness influence during hard machining of AISI 52100.

Thus, not only cutting forces, temperatures, chip thickness and geometry can be calculated, but finite element (FE) numerical simulations of hard machining can provide further insight into the behavior of the machining process such as grain size, hardness [21], residual stresses [22], phase transformation, etc.

Consequently, the aim of the present work is to give a contribution in FE analysis advance, validating a newly advanced FE model that includes temperature-dependent physical properties and workpiece microstructure data. The proposed phenomenological FE model is able to predict the complex thermo-mechanical history during hard machining of bearing steels and to distinguish the causes of microstructural changes between thermal and mechanical.

2. Experimental Procedure

The experimental data used for the analysis refer to those performed by Bedekar et al. [23] on hard turning of carburized SAE 8620 steel.

Rings of 285mm outer diameter, 245mm inner diameter and 38mm width were carburized and hardened (60/62HRC). Experiments were performed on a high precision horizontal CNC lathe, by using two low PCBN insert geometries - upsharp positive rake (UP) with a geometry of -20° rake angle and 50μm hone and honed negative rake (NH) with a geometry of +5° rake angle and 12μm hone – with two levels of wear conditions (VB=0μm (F-fresh) and VB=100μm (W-worn)) to produce white layers with different microstructures. Thus, the following tool geometry nomenclature was used: NH-W (Negative

Rake Worn Insert), NH-F (Negative Rake Fresh Insert), UP-W (Positive Rake Worn Insert) and UP-F (Positive Rake Fresh Insert). Insert wear was limited to 100μm to ensure low surface roughness.

Moreover, two values of cutting speeds (V=91m/min and V=273m/min) were investigated for a total of 8 different machining cases.

All experiments were carried out at constant depth of cut (DOP=100μm) and feed rate (f=50μm). Finally, the authors [23] analyzed microstructural changes by TEM and GAXRD and evaluated the nanohardness by nanoindentation tests.

3. Numerical Model

The commercial FE software DEFORM-2DTM (implicit solver) has been used to simulate the orthogonal cutting process of SAE 8620 steel (61HRC) using a plane–strain coupled thermo-mechanical analysis. An updated Lagrangian model with automatic remeshing technique is applied to achieve the mechanical and thermal steady state conditions during the simulation. Concerning the workpiece material, the isotropic hardening has been assumed and the workpiece was modeled as plastic divided into 10,000 isoparametric quadrilateral elements. The cutting tool, divided into 3500 elements, was modeled as rigid in the FE model. Moreover, a high mesh-density has been set and used for the workpiece.

To simulate the thermo-mechanical behavior of the current orthogonal cutting process, under severe plastic deformation (SPD) condition, the modified hardness-based flow stress model [20] was implemented. In particular, starting from the original J–C model Equation (1) it can be written as reported in Equation (2):

$$\sigma(\varepsilon, \dot{\varepsilon}, T)=[A+B\varepsilon^n] \times [1 + C \ln(\dot{\varepsilon}/\dot{\varepsilon}_0)] \times [1-((T-T_0)/(T_m- T_0))^m] \tag{1}$$

where A, B, n, C, and m are the material constants; ε is the equivalent plastic strain, $\dot{\varepsilon}$ and $\dot{\varepsilon}_0$ are the plastic strain rate and the reference plastic strain, respectively, T_0 is reference temperature and T_m is the melting temperature.

$$\sigma(\varepsilon, \dot{\varepsilon}, T, \Delta HRC, d)=B(T) \times (C\varepsilon^n + F + G\varepsilon) \times (1 + (\log(\dot{\varepsilon})^m-A)) \tag{2}$$

where B(T) takes into account the temperature effect, F and G consider the hardness influence, and the term $(1 + (\log(\dot{\varepsilon})^m-A))$ represents the strain rate impact.

The model proposed in this work starts from Equation (2) and modifies the constant C (MPa) of the flow stress to consider i) the grain refinement on the surface and subsurface caused by dynamic recrystallization (DRX), ii) the variation of the hardness and iii) the yield stress Equation (3):

$$C=a+(k/d\hat{~}0.5) \tag{3}$$

where d is the average grain size and a and k are two numerical constants. By this modification, the material flow stress is influenced by phase transformation (mainly thermally induced) and by dynamic events (mainly mechanically induced) that significantly modify the microstructure of the machined surface and subsurface during turning.

Thus, the thermo-mechanical behavior of the SAE 8620 steel is numerically represented by the new modified J–C law Equation (4):

$$\sigma(\varepsilon, \dot{\varepsilon}, T, \Delta HRC, d)=B(T) \times ((a + (k/d\hat{~}0.5)\varepsilon^n + F + G\varepsilon) \times (1 + (\log(\dot{\varepsilon})^m-A)) \tag{4}$$

The values of the numerical constants a, k, n, m, A and of the two hardness dependent factors F, G (Table 1) were calibrated through an iterative calibration strategy (Figure 1) according to what was available in the literature relating to the mechanical behavior of the material under investigation [20,24,25].

Table 1. Calibrated numerical constants and factors.

Description	Value
a	573
k	478
n	0.05
m	0.04
A	0.01
F	2.5*HRC-150
G	5*HRC-300
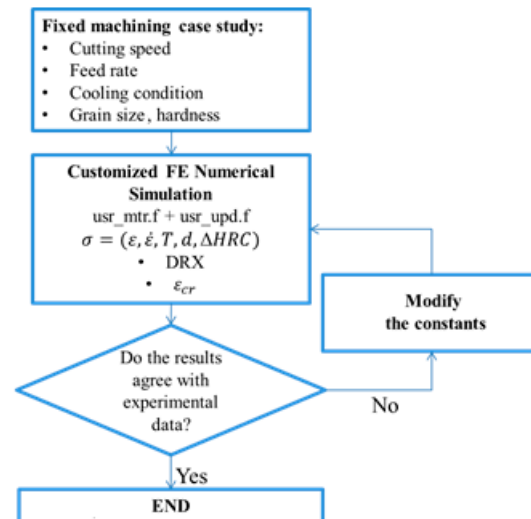
Figure 1. Iterative procedure to calibrate the constants.

The physical events influencing the mechanical properties, were predicted by implementing a user subroutine with the empirical relationships of Zener–Hollomon (Z–H) parameter for grain refinement and Hall–Petch (H–P) equation for hardness evolution [22]. In particular, all the constants related to DRX and hardness changes were calibrated for SAE 8620 steel following the calibration procedure reported in [26].

Figure 2 summarizes the FE strategy developed to properly simulate the microstructural alterations.

In particular, the newly developed FE model is able to predict thermal and mechanical events during hard machining, and to show, by their single contribution, when the microstructural changes are mainly thermally or mechanically induced.

In fact, considering the mechanical contribution to the DRX phenomenon, the user subroutine "SPD events" (Figure 2) determines the recrystallized grain size (through state variable model relating the initial grain size, material constant and the Z–H parameter) and evaluates the hardness variation according to H–P equation.

Concerning thermal contribution, the user subroutine "Thermal events" (Figure 2) evaluates the local temperature history in the deformation zone, chip and machined surface, and determines the phase transformation (based on an empirical formulation relating hardness variation to quenching and tempering phenomena).

As overall result, the FE model updates the machined material hardness considering both the mechanically and thermally-activated events causing respectively DRX and phase transformation phenomena.

Thus, such a model is able to evaluate and distinguish the single mechanical and thermal contribution taking place during the process showing the prevailing one and updating the material flow stress equation Equation (4).
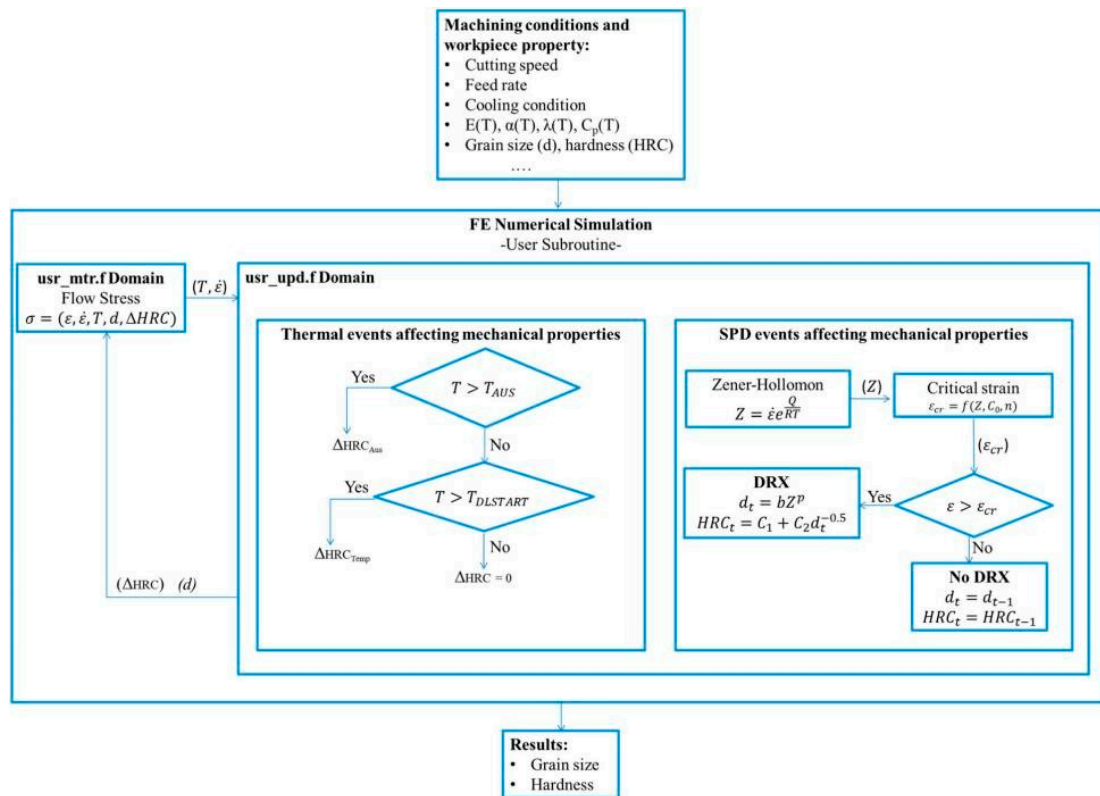
Figure 2. Finite element strategy to predict the grain size and hardness variation due to thermal and mechanical events.

4. FE Validation and Results

The proposed FE model was validated by comparing its output with the corresponding experimental data. Figure 3 shows that the implemented user routine gave stable and uniform data prediction in the steady-state zone. In particular, Figure 3 reports the numerical prediction for both grain refinement and affected layer at a cutting speed of V = 273 m/min and fresh insert with positive rake angle (UP-F).
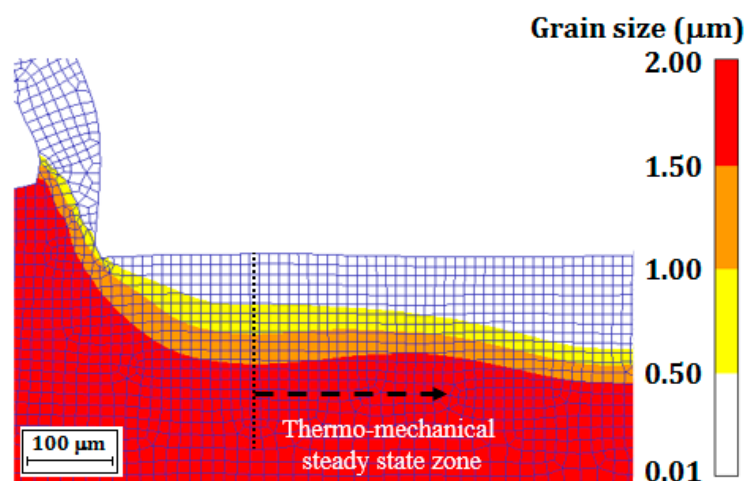
Figure 3. Grain size prediction: positive rake fresh insert with cutting speed (UP-F/V) = 273 m/min.

As reported in Figures 3–9, the results show the ability of the customized model to successfully predict the thermo-mechanical phenomena taking place during the selected processes.
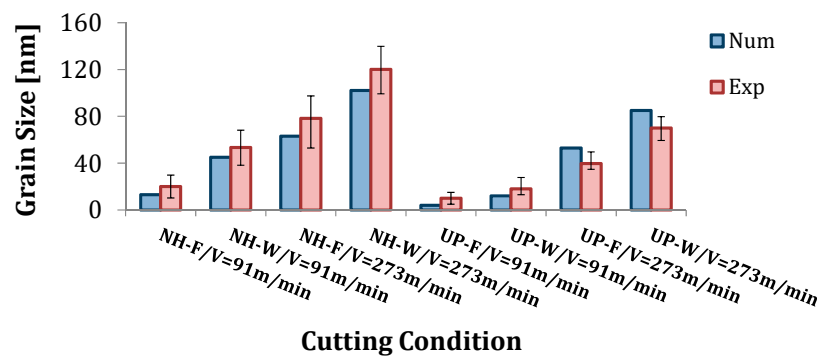
Figure 4. Grain size prediction: overall results (NH-W: negative rake worn insert, NH-F: negative rake fresh insert, UP-W: positive rake worn insert and UP-F: positive rake fresh insert).
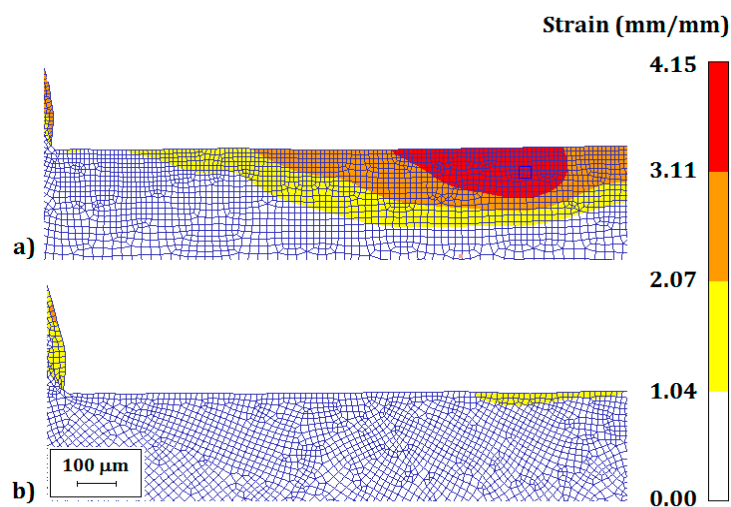

Figure 5. Prediction of strain distribution: (**a**) UP-F/V = 273 m/min, (**b**) UP-W/V = 273 m/min (UP-W: positive rake worn insert and UP-F: positive rake fresh insert).
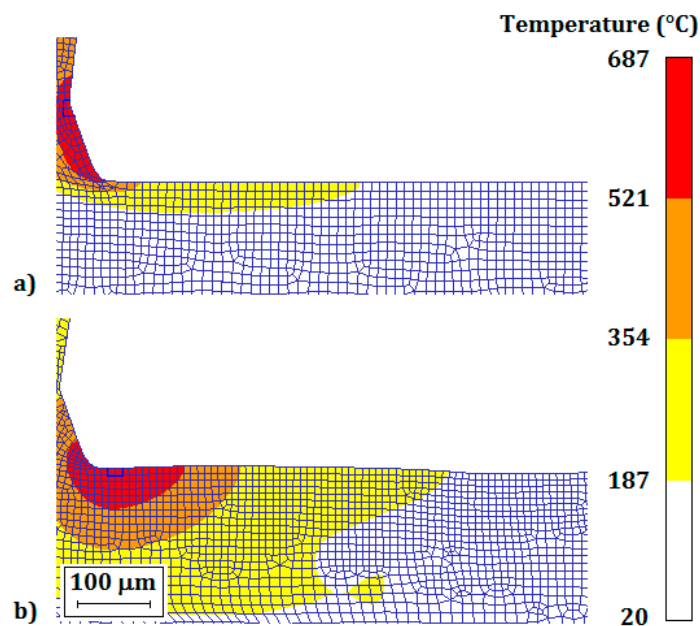

Figure 6. Prediction of temperature distribution: (**a**) NH-W/V = 91 m/min, (**b**) NH-W/V = 273 m/min (NH-W: negative rake worn insert).
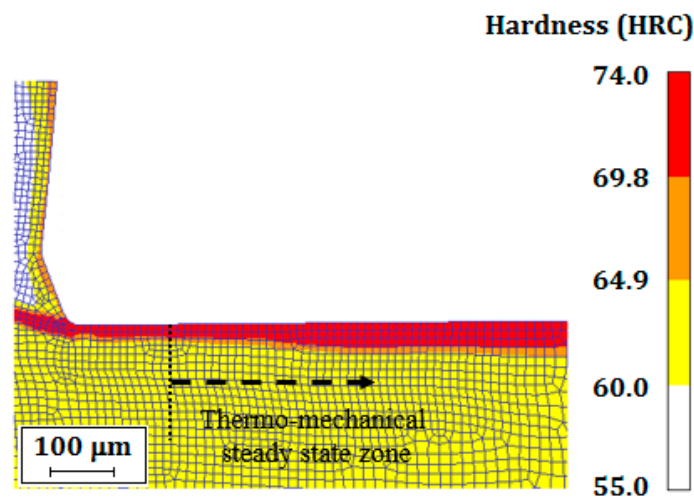
Figure 7. Hardness prediction: NH-W/V = 91 m/min (NH-W: negative rake worn insert).
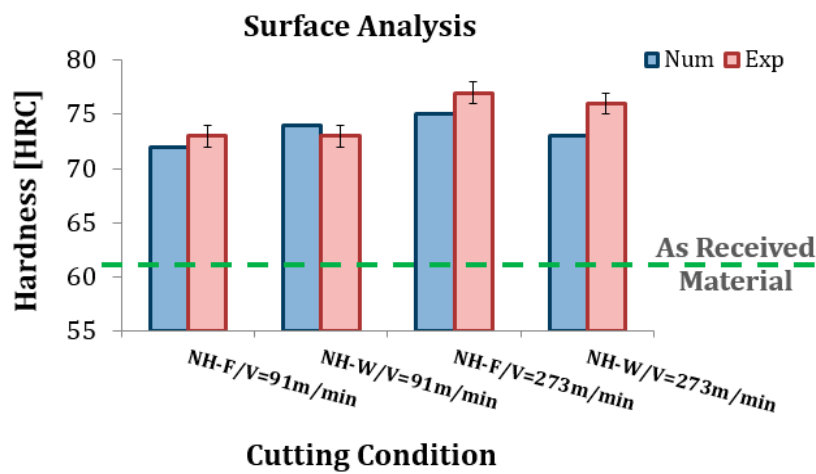

Figure 8. Surface hardness prediction (NH-W: negative rake worn insert, NH-F: negative rake fresh insert).
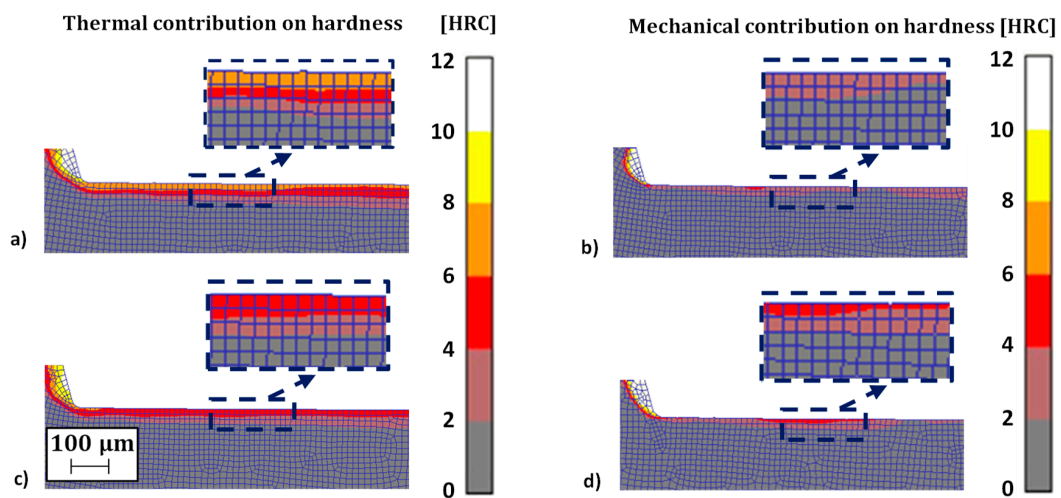

Figure 9. Thermal (phase transformation) and mechanical (dynamic recrystallization (DRX) event) hardness contribution to the as-received material hardness: a)–b) NH-W/V = 273m/min, c)–d) NH-F/V = 91m/min (NH-W: negative rake worn insert, NH-F: negative rake fresh insert).

Figure 4 reports the numerical–experimental comparison of all the analyzed tests, showing a good agreement in the prediction of the grain size evolution.

As experimentally found, the grain size range was about 100 times smaller than the bulk grain size (2 μm) [23].

For all the investigated cases, higher refinement (i.e., smaller grain size) was experimentally found by using a new cutting tool as shown in Figure 4. In these cases, FE model shows that, when hard machining is performed by a new cutting tool, higher strains provide smaller grain size due to grain refinement (Figure 5).

On the contrary, experiments show a grain size increase (i.e., coarser grain size) with the increase of the cutting speed (Figure 4). Thus, the FE model allows observation of increasing temperatures when the cutting speed rises, as seen in Figure 6.

For overall results, coarser grain size was produced on the machined surface and subsurface due to higher temperatures.

Figure 7 shows the hardness prediction when the cutting speed of V = 91m/min and worn insert with negative rake angle (NH-W) were used, while Figure 8 reports the comparison of surface hardness experimentally observed and numerically predicted.

A very good agreement between the numerical and experimental data was verified.

The numerical results confirm that machining of SAE 8620 hardened steel causes severe surface and subsurface structural changes, which are mainly thermally induced through phase transformations, as also suggested by the FE model.

In fact, the proposed phenomenological model makes possible to evaluate both thermally and mechanically induced microstructural changes and to show their single contribution in the deformation zone, chip and machined surface.

Hence, comparing NH-F (V = 91 m/min) and NH-W (V = 273 m/min) tests, a great difference is shown concerning grain size evolution (Figure 4), while a not evident difference is revealed concerning machined surface hardness variation (Figure 8).

This is due to the different mechanical and thermal events occurring for each single test. With the increase of the cutting speed, higher temperatures are reached during machining (Figure 6), resulting in a thermally-activated hardness increase for phase transformation phenomena (quenching). For this reason, although the test NH-W (V = 273m/min) was characterized by a coarser grain size (i.e., reduced mechanical influence on hardness increase), both compared tests showed the same machined surface hardness since a greater thermally induced phase transformation influence was registered at high cutting speeds (Figure 9).

Figure 9 shows the robustness of the proposed numerical model highlighting the single thermal and mechanical contributions to the hardness variation. As expected, for both the investigated cases, the thermal effect gave a greater contribution to the hardness increase than the mechanical one, demonstrating the predominant influence of phase transformation during hard machining of SAE 8620 steel.

Furthermore, the mechanical hardness contribution for the test NH-F (V = 91 m/min), due to grain refinement, was greater than the mechanical one registered for the test NH-W (273 m/min). This important finding is due to the combined effect of lower temperatures (i.e., reduced phase transformation) for lower cutting speeds (Figure 6) and smaller grain size when using a fresh insert (Figure 5): This numerical analysis gives a clear interpretation of the obtained results (Figure 8) and is helpful to understand the real physical meaning of the investigated process.

Figure 10 reports the hardness numerical profile from the machined surface to the bulk material. All the investigated cutting conditions highlighted a hardened layer of about 80 μm. Moreover, a good agreement between the prediction and the experimental evidences was recorded near to the machined surface (at 6 μm).
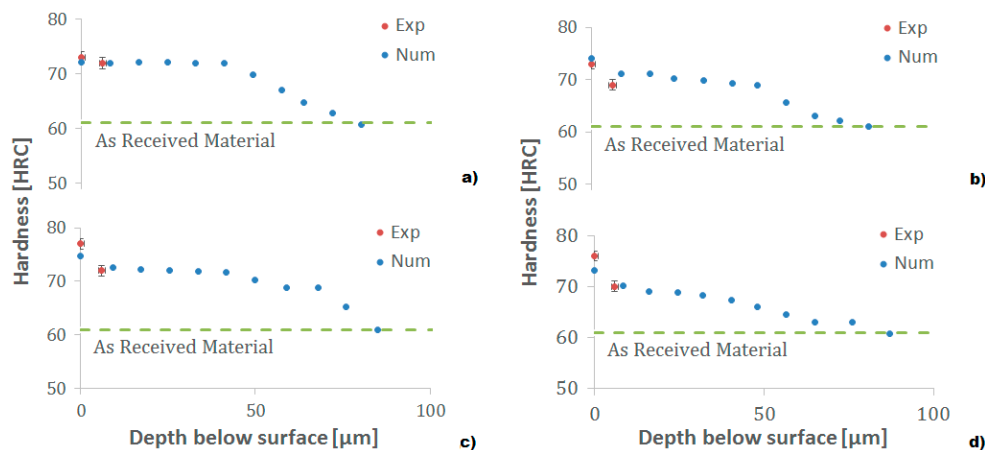
Figure 10. Hardness profile prediction: a) NH-F/V = 91m/min, b) NH-W/V = 91m/min, c) NH-F/V = 273m/min, d) NH-W/V = 273m/min (NH-W: negative rake worn insert, NH-F: negative rake fresh insert).

5. Discussion and Conclusions

In this paper, a FE model has been proposed to simulate the hard machining of SAE 8620 steel at varying cutting speed, insert geometry and flank wear. The proposed FE strategy successfully simulates both the thermal and the mechanical phenomena on the surface and subsurface leading to microstructural changes.

The Zener–Hollomon parameter and the Hall–Petch relation were implemented for predicting grain size and hardness evolutions. A new modified hardness-based J–C model was implemented considering the effect of grain size on the material's behavior during the SPD process. More specifically, the influence of grain refinement, due to DRX, on the material flow stress was taken into account following the Hall–Petch equation. This aspect is of main importance considering the inverse function existing between the flow stress curve and the grain size: smaller grain size (i.e., grain refinement) results in higher material strength.

The numerical results were validated by comparison with those performed by Bedekar et al. [23] and a satisfactory agreement was found. In particular the average error was always contained around 20% for grain size and 4% for the surface hardness.

Furthermore, it was found that the cutting speed, the insert geometry and the flank wear strongly influence the machined surface and subsurface integrity of SAE 8620 bearing steel.

In fact, with the increase of the cutting speed a coarser grain size was observed. In fact, at higher cutting temperatures the dynamic recrystallization is contained leading to a smaller amount of grain refinement. On the contrary, higher refinement is highlighted machining with fresh cutting tools which induce higher localized strains.

In particular, the developed FE model brought to observe that the hardness variation on the machined surface and subsurface is due to both mechanical and thermal contributions, showing a predominant thermal influence during hard machining.

The proposed phenomenological model allows better understanding of the physical aspects of the analyzed process, showing the contribution of the mechanically-activated hardness variation for DRX events and the thermally-activated hardness variation for phase transformation phenomena to the as-received material hardness.

The model highlights the influence of grain size and hardness variation on the material behavior at both macro and micro scale, directly considering the influence of microstructural changes on material flow stress also for higher strain rates and temperatures.

Thus, the proposed FE strategy can be used to properly simulate the cutting process of the SAE 8620 steel, providing accurate results since it was considered the coupled effect of grain refinement and microhardness variation on the material flow stress equation.

Conflicts of Interest: The authors declare no conflict of interest.

Nomenclature

A	adjustment factor
B	temperature-dependent factor
C	work-hardening coefficient
C_0	numerical constant
C_1	numerical constant
C_2	numerical constant
CNC	computer numerical controlled
DOP	depth of cut
PCBN	polycrystalline cubic boron nitride
DRX	dynamic recrystallization
F	hardness dependent factor
G	hardness dependent factor
GAXRD	glancing angle X-ray diffraction
H–P	Hall–Petch
ΔHRC	hardness modification
ΔHRC_{Aus}	hardness modification due to quenching
ΔHRC_{Temp}	hardness modification due to tempering
J–C	Johnson–Cook
Q	activation energy of material at high temperature
R	gas constant
SPD	severe plastic deformation
T	current temperature
T_{AUS}	austenite-start temperature
$T_{DLSTART}$	tempering-start temperature
T_{ROOM}	room temperature
TEM	transmission electron microscopy
V	cutting speed
VB	flank wear
Z	Zener–Hollomon parameter
Z–A	Zerilli–Harmstrong
Z–H	Zener–Hollomon
$\dot{\varepsilon}$	strain rate
ε	effective strain
ε_{cr}	critical strain
a	numerical constant
b	numerical constant
c	numerical constant
d	average grain size
d_{DRX}	recrystallized grain size
f	feed rate
k	numerical constant
m	numerical constant
n	numerical constant
p	numerical constant

References

1. The-Vinh, D.; Quang-Cherng, H. Optimization of Minimum Quantity Lubricant Conditions and Cutting Parameters in Hard Milling of AISI H13 Steel. *Appl. Sci.* **2016**, *6*, 83.
2. Huu-That, N.; Quang-Cherng, H. Surface Roughness Analysis in the Hard Milling of JIS SKD61 Alloy Steel. *Appl. Sci.* **2016**, *6*, 172.
3. Irfan, O.M.; Al-Mufadi, F.; Al-Shataif, Y.; Djavanroodi, F. Effect of Equal Channel Angular Pressing (ECAP) on Erosion-Corrosion of Pure Copper. *Appl. Sci.* **2017**, *7*, 1250.
4. Borislav, S.; Pavel, K.; Branislav, D.; Dragan, R.; Mirfad, T.; Michal, G. Application of an Adaptive "Neuro-Fuzzy" Inference System in Modeling Cutting Temperature during Hard Turning. *Appl. Sci.* **2019**, *9*, 3739.
5. Johnson, G.R.; Cook, W.H. A Constitutive Model and Data for Metals Subjected to Large Strains, High Strain Rates and Temperatures. *Proc. Seventh Int. Symp. Ballist.* **1983**, 541–547.
6. Calamaz, M.; Coupard, D.; Girot, F. A New Material Model for 2D Numerical Simulation of Serrated Chip Formation When Machining Titanium Alloy Ti–6Al–4V. *Int. J. Mach. Tools Manuf.* **2008**, *48*, 275–288. [CrossRef]
7. Childs, T.H.C.; Maekawa, K.; Obikawa, T.; Yamane, Y. *Metal. Machining: Theory and Applications*; Elsevier: Oxford, UK, 2000.
8. Man, X.; Ren, D.; Usui, S.; Johnson, C.; Marusich, T. Validation of Finite Element Cutting Force Prediction for End Milling. *Procedia CIRP* **2012**, *1*, 663–668. [CrossRef]
9. Zerilli, F.J. Dislocation Mechanics-based Constitutive Equations. *Metall. Mater. Trans. A* **2004**, *35*, 2547–2555. [CrossRef]
10. Guo, Y.B.; Wen, Q.; Woodbury, K.A. Dynamic Material Behavior Modeling Using Internal State Variable Plasticity and its Application in Hard Machining Simulations. *J. Manuf. Sci. Eng.* **2006**, *128*, 749–759. [CrossRef]
11. Follansbee, P.; Kocks, U. A Constitutive Description of the Deformation of Copper Based on the Use of the Mechanical Threshold Stress as an Internal State Variable. *Scr. Metall. Mater.* **1988**, *36*, 81–93. [CrossRef]
12. Yan, X.; Reiner, J.; Bacca, M.; Altintas, Y.; Vaziri, R. A Study of Energy Dissipating Mechanisms in Orthogonal Cutting of UD-CFRP Composites. *Compos. Struct.* **2019**, *220*, 460–472. [CrossRef]
13. Lin, Y.C.; Chen, X.M.; Liu, G. A Modified Johnson—Cook Model for Tensile Behaviors of Typical Hign—Strength Alloy Stell. *Mater. Sci. Eng. A* **2010**, *527*, 6980–6986. [CrossRef]
14. Ozel, T.; Ulutan. D. Prediction of Machining Induced Residual Stresses in Turning of Titanium and Nickel Based Alloys with Experiments and Finite Element Simulations. *Proc. CIRP Ann. Manuf. Technol.* **2012**, *61*, 547–550. [CrossRef]
15. Li, Z.X.; Zhana, M.; Fana, X.G.; Tana, J.Q. A Modified Johnson-Cook Model of as-Quenched AA2219 Considering Negative to Positive Strain Rate Sensitivities over a Wide Temperature Range. *Proc. Eng.* **2017**, *207*, 155–160. [CrossRef]
16. Le, C.; Changyu, Z.; Jian, P.; Jian, L.; Xiaohua, H. Fields–Backofen and a Modified Johnson-Cook Model for cp-ti at Ambient and Intermediate Temperature. *R. Metal. Mater. Eng.* **2017**, *46*, 1803–1809. [CrossRef]
17. Tan, Q.J.; Zhan, M.; Liu, S.; Huang, T.; Guo, J.; Yang, H. A Modified Johnson–Cook Model for Tensile Flow Behaviors of 7050-T7451 Aluminum Alloy at High Strain Rates. *Mater. Sci. Eng. A* **2015**, *631*, 214–219. [CrossRef]
18. Wang, X.; Huang, C.; Zou, B.; Liu, H.; Zhu, H.; Wang, J. Dynamic behavior and a modified Johnson–Cook constitutive model of Inconel 718 at high strain rate and elevated temperature. *Mater. Sci. Eng. A* **2013**, *580*, 385–390. [CrossRef]
19. Rotella, G.; Umbrello, D. Finite Element Modeling of Microstructural Changes in Dry and Cryogenic Cutting of Ti_6Al_4V Alloy. *Proc. CIRP Annals Manuf. Technol.* **2014**, *63*, 69–72. [CrossRef]
20. Umbrello, D.; Hua, J.; Shivpuri, R. Hardness-Based Flow Stress and Fracture Models for Numerical Simulation of Hard Machining AISI 52100 Bearing Steel. *Materials Sci. Eng. A* **2004**, *374*, 90–100. [CrossRef]
21. Caruso, S.; Imbrogno, S.; Rinaldi, S.; Umbrello, D. Finite Element Modeling of Microstructural Changes in Waspaloy Dry Machining. *Int. J. Adv. Manuf. Technol.* **2017**, *89*, 227–240. [CrossRef]
22. Madariaga, A.; Kortabarria, A.; Hormaetxe, E.; Garay, A.; Arrazola, P.J. Influence of Tool Wear on Residual Stresses When Turning Inconel 718. *Proc. CIRP* **2016**, *45*, 267–270. [CrossRef]

23. Bedekar, V.; Shivpuri, R.; Chaudhari, R.; Scott Hyde, R. Nanostructural Evolution of Hard Turning Layers in Response to Insert Geometry, Cutting Parameters and Material Microstructure. *Proc. CIRP Ann. Manuf. Technol.* **2013**, *62*, 63–66. [CrossRef]
24. Davis, J.R. (Ed.) *Metals Handbook*, 2nd ed.; ASM International: Cleveland, Ohio, USA, 1998.
25. Heat treating for the competitive edge, Modern steels and their properties, Akron steel treating company.
26. Umbrello, D.; Caruso, S.; Imbrogno, S. Finite Element Modelling of Microstructural Changes in Dry and Cryogenic Machining AISI 52100 Steel. *Mater. Sci. Technol.* **2016**, *32*, 1062–1070. [CrossRef]